Structural and Catalytic Characterization of the Mechanism and Site Requirements in Fe-Catalyzed Fischer-Tropsch Synthesis

Enrique Iglesia, Anwu Li, Mai Tu, Senzi Li, Wei, Li

University of California

Department of Chemical Engineering

Berkeley, CA 94720

I. FISCHER-TROPSCH SYNTHESIS ON IRON CATALYSTS

1. Introduction

1.1. Structure and Function of Active Phases

Fe-based oxides have been used as commercial catalysts for Fischer-Tropsch synthesis (FTS) to produce a large variety of paraffin and olefin products, ranging from methane to high molecular weight waxes [1]. During activation by synthesis gas and subsequent FTS reaction, several phases including metallic iron, iron carbides and iron oxides are known to co-exist at steady-state conditions [2-5]. The distribution and amounts of these phases depend on exposure to various activation and reaction conditions, leading to different catalytic performances in FTS. Some researchers [6] have proposed that surface iron atoms are responsible for FTS activity, while some others considered surface carbides or a mixture of carbides [7,8] and metallic iron [9] to be the active phase. There are also some reports that suggest that magnetite Fe_3O_4 is the active phase in FTS [10-12]. Although these studies have each provided some evidence to support their specific proposals about the active phase, the available information remains phenomenological, and a method to identify the active phase during reaction and to count the number of active sites has not yet been established.

Based on our previous research on Co [13,14] and Fe catalysts [15,16] for FTS, our first characterization step involves temperature-programmed reactions of Fe-based catalysts with flowing streams of H_2, CO and a H_2-CO mixture. We monitored the gas phase concentrations throughout the reduction and carburization processes by means of an on-line mass spectrometer, and followed the evolution of bulk phases and crystal size by X-ray diffraction and of surface area by nitrogen physisorption measurements. In this way, we can determine the temperature required for the formation of Fe carbides as well as the stoichiometry and structure of such carbides. Our goal is to develop a new synthesis method to improve the compositional and structural purity of Fe carbides formed, and consequently to refine the structure-function relationships that we have previously proposed to interpret the catalytic behavior of Fe-based catalysts.

1.2. Effect of Zn, K and Cu

Many components have been added to Fe catalysts in order to improve their mechanical and catalytic properties. Our previous studies have shown that zinc, alkali and copper [16,17] promote the catalytic properties of Fe oxides. Zinc oxide, as a non-reducible oxide in FTS conditions, appears to stabilize the surface area of Fe oxide. Alkali, as a modifier of the adsorption enthalpies of H_2 and CO, increases the selectivity to desired C_{5+} products. Copper promotes the carburization processes and decreases the temperature required for the activation of iron oxide. Here, our initial efforts have focused on Fe-Zn-K-Cu catalysts. We have prepared a series of Zn and Fe co-precipitated oxides with varied Zn/Fe ratios and then introduced varying amounts of K and Cu. We are examining the surface area, bulk structure, required reduction and carburization temperatures as well as the catalytic behavior of these catalysts, in order

to identify optimum Zn/Fe ratios and Cu and K contents that give maximum site density and catalytic activity.

2. Synthesis Procedures for Fe-Zn-K-Cu Samples

All catalysts were prepared by co-precipitation of zinc and iron nitrates at a constant pH of 7.0 in order to form porous mixed oxides. Then, these oxide precursors were impregnated with an aqueous solution of potassium and copper salts using incipient wetness methods. The Zn/Fe oxide precursors were prepared first. Fe nitrate (1.4 M) and Zn nitrate (3.0 M) solutions were mixed at a given atomic Zn/Fe ratio. A solution of ammonium carbonate (1 M) was prepared separately. Deionized water (ca. 50 ml) was added into a large flask, which was heated on a hot plate with a magnetic stirrer and held at 80^{o}C throughout the preparation process. The mixed Zn/Fe solution was added at 2 cm^{3}/min flow into the flask through a feeding pump. At the same time, the ammonium carbonate solution was fed separately, and its flow was controlled to maintain the slurry pH at 7±0.1, as monitored by a pH meter. The resulting precipitates were washed several times with about 1 *l* water per gram catalyst, dried at 120^{o}C overnight, and then calcined at 350^{o}C for 1 h. The calcined material was promoted with 2 at.% K using K_2CO_3 solution (0.16 M) by incipient wetness and then dried. The same process was repeated in order to promote samples with 1 at.% Cu using $Cu(NO_3)_2$ solution (0.16 M). Finally, the dried material was treated in dry air at 400^{o}C for 4 h. This final calcination temperature was chosen from temperature-programmed oxidation data that show that this temperature is sufficient to decompose all metal nitrates and carbonates except K_2CO_3. The catalysts contain CuO, ZnO, Fe_2O_3 and K_2CO_3. These catalysts were pressed at 443 MPa into pellets, lightly crushed, and then sieved to retain the 80 - 140 mesh fraction for FTS reaction.

3. Catalyst Characterization

3.1. Protocols for the Characterization of Fe-based FTS Catalysts

This research program addresses the synthesis and the structural and catalytic characterization of the active sites of Fe-based catalysts for FTS. We have designed a matrix of samples that contains a systematic range of multi-components catalysts in order to determine the number and type of surface sites present on fresh catalysts and the samples after FTS reaction (Table 1). Our objective is to develop rigorous relationships between the synthesis methods, the resulting catalyst structures, and their function in FTS reactions.

3.2. Crystal Structure

Powder X-ray diffraction (XRD) measurements (Siemens D-5000, Cu Kα radiation) show that a rhombohedral corundum-type hematite Fe_2O_3 forms in samples with Zn/Fe ratios less than 0.2, and that a cubic spinel-type franklinite $ZnFe_2O_4$ forms in the sample with a Zn/Fe ratio of 0.4. In intermediate compositions, both Fe_2O_3 and $ZnFe_2O_4$ phases are detected (Figure 1).

At lower Zn/Fe ratios (0.05 and 0.1), Zn appears to exist as an amorphous phase of $ZnFe_2O_4$. At higher Zn/Fe ratio (0.4), $ZnFe_2O_4$ is the only detectable bulk phase, but there must be certain amount of Fe present in an amorphous Fe_2O_3 form since the stoichiometric Fe/Zn ratio in $ZnFe_2O_4$ is 0.5. The impregnation of potassium and copper and the subsequent calcination do not influence the detected bulk phases; therefore, their XRD patterns are omitted here.

3.3. Surface Area

The surface area measurements were conducted on an automated six-station Quantachrome adsorption apparatus using the BET method. The results are

summarized in Table 2. Pure Fe_2O_3 prepared by a co-precipitation method and subsequent calcination at a low temperature (350^{o}C) has a surface area of 100 m^2g^{-1}. Addition of less than 10 at. % Zn (Zn/Fe ratio = 0.05, 0.1) leads to a decrease in surface area. At higher Zn/Fe ratios (>0.2), $ZnFe_2O_4$ structures form and the surface area increases to values similar to those on pure Fe_2O_3. At the high calcination temperature (400^{o}C) required to decompose carbonate and nitrate precursors, the addition of Zn, however, significantly stabilizes the surface areas at all Zn loadings. The surface area of the sample with a Zn/Fe ratio of 0.4 is almost twice that of the Zn-free catalyst (96 vs 53 m^2g^{-1}). It appears that the $ZnFe_2O_4$ phase resists sintering during calcination at higher temperatures. The effect of $ZnFe_2O_4$ as a structural promoter becomes increasingly critical as the required calcination temperature increases. The minimum ratio of Zn/Fe required to inhibit catalyst sintering is about 0.2, which appears to coincide with the compositional range required to form $ZnFe_2O_4$ crystallites.

3.4. Temperature-Programmed Surface Reaction (TPSR) of Fe_2O_3 in H_2 and in a Mixture of $CH_4/4H_2$

3.4.1 TPSR Unit and Experimental Procedures

A schematic diagram of the TPSR unit is given in Appendix 2.1. A series of gas purifiers, five mass flow controllers (MFC) and various valves mounted on an aluminum panel allow us to introduce all the necessary reactive gases or gas mixtures into the reactor. A 4-port valve and a 6-port valve controlled by a digital pulse generator (Valco Instruments Co., Inc.) was used to purge or change the gas flow in isotopic switch and pulse studies. Typically, a 0.2 g sample was charged into a quartz microreactor with 10 mm I.D. containing a quartz frit. Samples were heated in a flowing air stream (100 cm^3/min 20% O_2 in Ar) at a rate of 20^{o}C/min to the calcination temperature of 400^{o}C.

The temperature was maintained at 400^{o}C for 15 minutes until all adsorbed water and CO_2 were removed. Then, the reactor was cooled down to ambient temperature. A flow of 20% H_2 or CH_4/4H_2 mixture balanced by 80% Ar (Ar is used as an internal standard) was introduced at a flow rate of 100 cm^3/min into the reactor. The temperature of the furnace was maintained by a temperature-programmed controller and increased at a ramping rate of 10^{o}C/min. A 1/16" stainless steel tube connected to the vacuum chamber of a mass spectrometer (Leybold Inficon Instruments Co., Inc.) was inserted into the outlet end of the reactor to divert a portion of effluent gases for mass spectroscopic analyses. The reactor effluent lines leading to the mass spectrometer were maintained at 125^{o}C in order to prevent condensation of reactants or products.

3.4.2. TPSR of Fe_2O_3 in H_2

Figure 2 shows the rate of H_2O evolution during the reduction of Fe_2O_3 powder (MCB, 99%, BET surface area 7 m^2g^{-1}) in H_2 flow. The ratio of the areas under the two H_2O peaks is about 1:8, indicating that the reduction of Fe_2O_3 occurs in two steps, i.e., Fe_2O_3 is first reduced to Fe_3O_4 between 300 ~ 380^{o}C, and then to metallic Fe. XRD measurements confirm the formation of Fe_3O_4 at the first step of reduction and of metallic Fe at the end of second reduction peak.

3.4.3. TPSR of Fe_2O_3 in $CH_4/4H_2$

Figure 3 shows the CH_4 consumption and the H_2O formation rate during reduction/carburization of Fe_2O_3 (MCB, 99%) in a gas mixture of $CH_4/4H_2$. The H_2O trace is similar to that measured during H_2 TPR. XRD measurements show Fe_3O_4 forms in the first step and metallic Fe in the second step. Neither bulk carbides nor graphite were detected by XRD throughout the reaction. A small amount of CH_4 (240 μmol) is consumed in the second step of the reaction. Also, trace amounts of CO and CO_2 (total carbon amount of 40 μmol) form at higher temperatures of the reduction/carburization process, apparently as a result of the reduction of residual Fe oxides by methane. About 200 μmol of carbon (1 mmol carbon/g-cat) residues remain in the samples. The ratio of oxygen removed in the form of water to iron is about 1.44, and the ratio of residual carbon to Fe is 0.07. This indicates that most of oxygen is removed by H_2 rather than by methane. Therefore, the carbon residues in the sample either incorporate with Fe forming amorphous carbides or deposit on the surface. The significant amount of Fe metal produced and the small amount of residual carbon indicates that Fe_2O_3 is reduced to metallic Fe prior to carburization to carbides, and that the diffusion of carbon into the compact iron crystallite to form Fe_xC is slow and incomplete.

3.4.4. Thermodynamic Phase Diagram for Fe_3C-Fe-C System

Figure 4 shows the equilibrium relationships for Fe metal and Fe_3C in contact with CH_4 and H_2 at a given gas composition and temperature. There is a narrow region (an area below the solid line and above the dotted line with the CH_4 concentration between 0 ~ 25 % and the temperature between 600 ~ 1000^{o}C), in which Fe_3C can be formed without significant contamination by graphite. According to this phase diagram,

carburization of Fe oxides with a CH_4/H_2 mixture would lead to the formation of oxygen-free and graphite-free carbides, if controlled within this very narrow temperature and composition range. The TPR results by reaction with $CH_4/4H_2$ (Figure 3) indicate that Fe oxide is reduced by methane only at higher temperatures while the formation of carbide is significantly restricted by the diffusion rate of carbon at the temperature required by thermodynamics for Fe_3C.

3.5. Temperature-Programmed Reduction (TPR) of Fe-Zn and Fe-Zn-K-Cu Samples in H_2

3.5.1. TPR Unit and Experimental Procedures

Temperature-programmed reduction (TPR) of metal oxides in a H_2-containing stream can be used to measure the reaction rate and oxygen content in reducible metal oxides. In our study, the TPR experiments were carried out using a Quantasorb (Quantachrome) unit (Appendix 2.2) coupled with a programmable furnace. Typically, a 0.03 g sample was loaded within the bottom of a U-type quartz tube cell (4 mm I.D.) containing a thermowell in direct contact with the sample bed. A gas mixture of 20% H_2 in Ar was passed through the reference side of a thermal conductivity detector (TCD), and then introduced into the reactor cell. The gas flow rate was measured and controlled by an electronic mass flow meter (Porter Instruments Inc.) Before thermal conductivity measurements, the water produced was removed using a molecular sieve trap (Aldrich, 13X) placed in the effluent stream. The dried gas phase products then flowed through the sample side of the TCD. The sample temperature and the difference in thermal conductivity signals between the two sides was recorded and processed using Labview software. CuO was used as the standard in order to calibrate the sensitivity of the TCD to H_2 concentration. The TCD current was set at 150 mA.

3.5.2. TPR of Fe, Zn and Cu Oxides in H_2

TPR of bulk Fe_2O_3, ZnO and CuO were used as references in order to identify the reduction of individual metal oxide in multi-component metal oxides. Figure 5 shows the TPR of Fe, Zn, Cu oxides in H_2. Bulk CuO starts to reduce at much lower temperatures than the other oxides. Fe_2O_3 reduces between 200 ~ 600^{o}C. ZnO begins to reduce to Zn metal at 550^{o}C and rapidly sublimes.

3.5.3. TPR of Fe-Zn and Fe-Zn-K-Cu Samples in H_2

Figure 6 shows the oxygen removal rates on Fe-Zn precursors and Fe-Zn-K-Cu samples in H_2. Fe-Zn samples (solid lines) react rapidly with H_2 to form Fe_3O_4. When the sample reaches the stoichiometry of Fe_3O_4, the reduction rate decreases sharply. Further reduction produces metallic Fe. Addition of Zn in Fe appears not to influence the reduction of Fe oxides even at higher Zn loadings (>0.2) where $ZnFe_2O_4$ is the only bulk phase. This indicates that $ZnFe_2O_4$ structure, rather than stabilizing the surface area, collapses as soon as Fe oxides are reduced. Fe-Zn-K-Cu samples (dotted lines), initiate the reduction with H_2 at much lower temperatures at all Zn loadings, but finish the reduction at higher temperatures than those samples without K and Cu. The entire reduction appears to be prolonged over both initial and final processes by the addition of Cu and K. Here, the first step reduction is separated into two parts, some move to lower temperatures (ca. 200^{o}C), at which CuO is reduced, while some are retained and reduced at the same temperature as those samples without K and Cu. Since H_2 can dissociatively adsorb on Cu, those Fe oxide crystallites that are in contact with Cu can be readily reduced as soon as CuO is reduced. Fe oxide crystallites that are not near Cu, will not benefit from the dissociated hydrogen, and therefore will not reduce at low temperatures. In contrast with Cu, which acts to lower the reduction temperature, K

apparently inhabits reduction processes. The inhibition effect of K on the reduction of Fe oxides in H_2 appears to be weaker at higher Zn loadings. This may probably be due to the fact that Zn oxides are able to hold K from Fe oxides. In summary, the addition of Zn does not influence the reduction of Fe oxides; Cu decreases the reduction temperature while K inhibits the reduction of Fe oxides in H_2.

3.6. Isotopic Tracer Studies on FTS Catalysts

This part of the project involves developing a mathematical model for the isotopic switch experiments we plan to carry out to characterize the active sites of FTS catalysts. In an isotopic switch experiment, the isotopic composition of the reactants is abruptly changed, but the chemical composition does not change, leading to unperturbed chemical reactions if no significant kinetic isotope effects are present. During the experiment, the steady state or equilibrium is not disturbed and the experiment can be carried out during chemical reactions. The relaxation and evolution of the labeled compound are continuously monitored by mass spectrometry, and the curves provide information on the number and kinetic properties of the active sites. The area under the relaxation curve gives the total number of kinetically available sites, and the shape of the curve provides information about the kinetic behavior of the sites. This method has been recently used in our group to determine the number and strength of basic sites on oxide catalysts by carrying out a $^{13}CO_2/^{12}CO_2$ switch [18].

The determination of the total number of sites from the area is straightforward. The shape analysis of the curve to obtain the kinetic parameters, however, is rather complicated because of the non-uniformity of the sites and of the effect of readsorption of the reactants. In this work, we are developing a mathematical method to deconvolute the relaxation curve by using multi-compartment description of surface sites and by

rigorously taking into account the effect of readsorption. The mathematical model includes a set of differential equations describing the mass balance of the gas phase and each surface compartment.

For the gas phase: $$-V\frac{dC^{13}}{dt} - mN_s\sum_i\left(x_i\frac{d\theta_i^{13}}{dt}\right) = FC^{13}$$

For each compartment: $$-\frac{d\theta_i^{13}}{dt} = -\frac{k_{ai}}{1+K_iC_0}C^{13} + k_{di}\theta_i^{13}$$

Here k_{ai}, k_{di} and x_i are the adsorption, desorption rate constant, and the fraction of the surface sites for the ith compartment, respectively, and they are the parameters to be determined from the experiment concentration curve C^{13} versus time. The differential equations are solved numerically for a given set of kinetic parameters, and the parameters are optimized by minimizing the difference between the calculated and experimentally measured C^{13} values. Currently the algorithm and computer programs are under development. The developed programs will be used to analyze transient isotopic measurements of the number of sites and the FT mechanism. The isotopic transients will include switching from ^{13}CO to ^{12}CO, H_2 to D_2, and H_2O to D_2O during reactions of synthesis gas on Co and Fe catalysts.

4. Fischer-Tropsch Synthesis on Fe-based Catalyst in Fixed-bed Reactor

4.1. Catalytic Microreactor Unit (CMRU) for Fischer-Tropsch Synthesis

4.1.1. Brief Description and Schematic Diagram of Catalytic Microreactor Unit

Fischer-Tropsch synthesis was performed in a fixed-bed, single-pass flow reactor, hereafter referred to as the Catalytic Microreactor Unit (CMRU) (Appendix 2.3). Synthesis gas was introduced as H_2/CO mixtures using N_2 as an internal standard. Synthesis gas H_2/CO/N_2 (Altair: 99.9% H_2, 99.9% CO, 99.99% N_2) was fed as a 62/31/7 mol% mixture and passed through Sorb-Tech RL-13 activated carbon in order to remove metal carbonyls. All feed streams passed through gas purifiers (Matheson, Model 452:4A molecular sieve) in order to remove water.

Gas flows were metered using mass flow controllers (Porter, Model 201-AFASVCAA) and an interface module (Porter, Model CM-4). All flow controllers were calibrated for an outlet pressure of 20 atm and for a pressure drop of 15 atm across the meter. The three-zone ATS 302C Series 3210 split tube furnace was controlled with three temperature controllers (Watlow, Series 982 and 988). Total system pressure was maintained using a dome-loaded back-pressure regulator (Mity Mite Model S-91xw).

Heat tracing of lines to 160~180^{o}C started at the end of reactor (Appendix 2.3). Tubular reactors were constructed of stainless steel (304, ½"×0.028") and included a pre-heat tube (1/4"×0.028). The pre-heat tube was put into furnace to pre-heat feed gases. There was a stainless steel (volume 75 ml) trap below the reactor. The temperature of the trap was maintained at 145^{o}C in order to collect liquids. After the reaction reached steady state at a given set of conditions, the sample collected for the first 12 h from trap was discarded. The sample for the following 12-24 h was collected and saved for subsequent analysis by gas chromatography.

The feed gas and reactor effluent were analyzed on-line using a gas chromatograph (Hewlett Packard, Model 5890 Series II) equipped with a 10-port sampling valve and two sample loops. One sample loop was injected into a HP-1 capillary column (crosslinked methyl silicone, 50 m × 0.32 mm × 1.05 µm) while the other was injected into a Porapak Q (6"×1/8") packed column. A thermal conductivity detector (TCD) was used to analyze Ar, N_2, CO, CO_2, and light hydrocarbons eluting from the packed column. A flame ionization detector (FID) analyzed all products except for Ar, N_2, CO, CO_2, and the water eluting from the capillary column. Separation of components was accomplished using GC procedures described in the Appendix 3.1. The reactor effluent, when not injected into the GC columns, passed through a sample port to enable syringe extraction for mass spectroscopic (MS) analysis and through a cooled trap for the collection of condensable products for more detailed off-line GC and MS analysis.

4.1.2. Catalyst Loading and Activation

The Fe-based catalyst (80-140 mesh, 0.4 g) was diluted with quartz chips in order to avoid temperature gradients. The quartz chips were washed with diluted nitric acid and calcined at 600^{o}C. The total bed volume, including catalyst and quartz chips, was 8 cm^3 to give a bed height about 8 cm. Temperatures were recorded along the catalyst bed during FT synthesis. It was found that temperatures were within ±0.5^{o}C of the average axial temperature and at any axial position, they were within ±0.2^{o}C of the desired temperature. For all runs, the catalyst was activated before FT synthesis reaction. The activation was carried out in-situ by heating the catalyst in synthesis gas at 1 atm by increasing the temperature from 20^{o}C to 270^{o}C at a rate of 1^{o}C/min. After

holding it at 270°C for about 0.5 h, the reactor temperature and pressure were set at the desired reaction conditions.

4.2. Certification of the Catalytic Microreactor Unit

FT synthesis rates and selectivities were measured on the catalyst (Zn/Fe = 0.07, 2 at.% K, 1 at.% Cu) in order to compare with literature results and thus to certify reactor operation, data acquisition, and data analysis procedures. This particular catalyst was used for CMRU certification because data are available on this catalyst [16] (Table 3) and on similar catalysts. The comparison of our results to those of the catalyst served to verify selectivity and rate calculations and certified absolute detector response factors for the major products on FT synthesis reactions. This catalyst was run at 5 atm and 270°C. The results were listed in Table 3 and compared with literature data [16]. The results are in excellent agreement with the literature data [16].

4.3. Fischer-Tropsch Synthesis on Zn/Fe (0.07) and CO_2 Effects

A catalyst with an atomic Zn/Fe ratio of 0.07 was used for FTS at 235°C and 21.4 atm. This catalyst was prepared by constant pH co-precipitation methods and it was promoted by impregnation with 2 at.% K and 1 at.% Cu.

Figures 7 and 8 show CO conversion and CO_2, CH_4 and C_{5+} selectivities as a function of time on stream, respectively. It is seen that methane selectivity was low and C_{5+} selectivity was as high as 84% on this catalyst at these reaction conditions.

Figures 9 and 10 show chain formation probability (carbon selectivity (%)/carbon number) and α-olefin/n-paraffin ratio as a function of carbon number, respectively. Hydrocarbon selectivity decreased with carbon number because of the increasing probability for olefin readsorption and chain initiation as the larger olefins face more severe transport restrictions as they are removed from catalyst pores.

The effects of CO_2 addition on the rate of water-gas shift reaction rates and on CO_2 selectivity were investigated by adding CO_2 at 235^{o}C and 21.4 atm synthesis gas. The partial pressure of synthesis gas maintained constant as the CO_2 pressure was varied. Table 4 also shows CO_2 addition results. It is found that CO_2 addition did not influence FTS reaction rates. CO_2 addition decreased the net CO_2 selectivity (defined as the percentage of the converted CO appearing as CO_2) by decreasing the net rate of water-gas shift. In contrast, CO conversion rate to hydrocarbons increased with the added CO_2 partial pressure. This is expected if CO conversion remained almost unchanged and CO_2 selectivity decreased with CO_2 partial pressure. However, even when CO_2 partial pressure was 8 atm, some CO_2 was produced during FTS reactions. This is in agreement with our calculations, which indicate that at these reaction conditions and 26% CO conversion, a CO_2/CO ratio of about 15 in the feed (e.g. CO_2 partial pressure about 100 atm) would be required in order to avoid any net CO_2 formation via water-gas shift reactions. It shows that although CO_2 addition can be used to decrease CO_2 yields during FTS, the elimination of net CO_2 formation may well require levels of CO_2 that are impractical because of separation and re-compression costs.

4.4. Fischer-Tropsch Synthesis over Zn/Fe (0.1) under Various Conditions

FT synthesis on a Zn/Fe (0.1) catalyst was examined at various temperatures and pressures. Figure 11 shows CO conversion as a function of reciprocal space velocity under different conditions. Water-gas shift reactions during FT synthesis lead to a reduced water concentration and an increased hydrogen concentration, both of which increase CO conversion rate [19]. Therefore, CO reaction rate was almost independent of space times at 220^{o}C and 235^{o}C. Figs. 12, 13, 14 show CO_2 and hydrocarbon

selectivities as a function of CO conversion. CO_2 selectivity increased with CO conversion at all conditions. High temperatures favored CO_2 and methane formation. Low temperatures favored the formation of high molecular weight hydrocarbon.

CO conversion rate and selectivities were further compared at similar CO conversion at all reaction conditions. The results were listed in Table 5. It also shows that low temperatures and high pressures favor the formation of higher molecular weight hydrocarbons. Both CO_2 selectivity and the olefin content increase as the reaction temperature increases. It appears as if low temperatures and high pressures increase the probability of olefin readsorption and chain growth, which leads to their desorption as paraffins and to a lower olefin selectivity. Reaction rates on Fe-Zn-Cu-K catalysts are similar to those obtained on Co-based when the differences in reaction temperatures are taken into account. Co-based catalysts are limited, however, to operation at low temperatures, because they produce predominantly C_1-C_{10} hydrocarbons and high methane selectivities above 230-240^{o}C.

References

1. M. E. Dry, The Fisher-Tropsch Synthesis, in *Catalysis-Science and Technology*, Vol. 1, p. 160, J. R. Anderson and M. Boudart eds., Springer Verlag, New York, 1981.
2. F. Fischer and H. Tropsch, *Brennstoff-Chem.* **7** (1926) 97.
3. R. B. Anderson, in *Catalysis* Vol. 4, p. 29, P. H. Emmett eds., Van Nostrand-Reinhold, New York, 1956.
4. H. H. Storch, N. Golumbic and R. B. Anderson, *The Fischer-Tropsch and Related Syntheses*, Wiley, New York, 1951; R. B. Anderson, *The Fischer-Tropsch Synthesis*, Wiley, New York, 1984.

5. H. Kolbel and M. Ralek, *Catal. Rev.-Sci. Eng.* **21** (1980) 225.

6. J. W. Niemantsverdriet and A. M. van der Kraan, *J. Catal.* **72** (1981) 385.

7. J. A. Amelse, J. B. Butt and L. J. Schwartz, *J. Phys. Chem.* **82** (1978) 558.

8. G. B. Raupp and W. N. Delgass, *J. Catal.* **58** (1979) 348.

9. R. Dictor and A. T. Bell, *J. Catal.* **97** (1986) 121.

10. J. P. Reymond, P. Meriaudeau and S. J. Teichner, *J. Catal.* **75** (1982) 39.

11. C. S. Kuivila, P. C. Stair and J. B. Butt, *J. Catal.* **118** (1989) 299.

12. C. S. Huang, L. Xu and B. H. Davis, *Fuel Sci. Tech. Int.* **11** (1993) 639.

13. E. Iglesia, and S. C. Reyes, R. J. Madon and S. L. Soled, *Advances in Catalysis*, Vol. 39, p. 221, Academic Press, 1993.

14. E. Iglesia, *Appl. Catal. A: General* **161** (1997) 59.

15. S. Soled, E. Iglesia and R. A. Fiato, *Catal. Lett.* **7** (1990) 271.

16. S. Soled, E. Iglesia, S. Miseo, B. A. DeRites and R. A. Fiato, *Topics in Catal.* **2** (1995) 193.

17. E. Iglesia, A research proposal submitted to the Division of Fossil Energy.

18. M. T. Xu, E. Iglesia, *J. Phys. Chem. B* **102(6)**, 961-966, 1998.

19. A. P. Raje, R. J. O'Brien and B. H. Davis, *J. Catal.* **180** (1998) 36.

Table 1 Matrix of Fe-Zn-K-Cu Samples and Characterization Methods for FTS Reaction				
Composition of the Catalysts			Characterization Before and After FTS	FTS Reaction
Zn/Fe Mole Ratio	K (atom%)	Cu (atom%)		
0	0	0	XRD Surface Area In-Situ XAS H_2-TPR CO-TPR H_2-TPR O_2-TPR (H_2+CO)-TPR H_2-TPR O_2-TPR	Effect of Reaction Condition 220°C 21.4 atm 235°C 21.4 atm 270°C 5 atm Effect of CO_2 addition
		1		
	2	0		
		1		
		4		
	4	1		
0.05	0	0		
	2	1		
	4	4		
0.1	0	0		
		4		
	2	0		
		1		
		4		

Table 1 Matrix of Fe-Zn-K-Cu Samples and Characterization Methods for FTS Reaction				
	4	1		
0.2	0	0		
	2	1		
	4	4		
0.4	0	0		
		1		
	2	0		
		1		
		4		
	6	1		

Table 2 Surface Areas (m_2g_{-1}) of Fe-Zn and Fe-Zn-K-Cu Samples					
Zn/Fe Mole Ratio	0	0.05	0.1	0.2	0.4
Fe-Zn	100	83	82	100	111
Fe-Zn-K-Cu	53	56	53	75	96

Table 3

The Fischer-Tropsch Synthesis Results on the Sample (Zn/Fe = 0.07, 2 atomic % K, 1 atomic % Cu)

	Results by CMRU	Results in Literature [16]
Catalyst weight (g)	0.4	2.5
Temperature (^oC)	270	270
Pressure (atm)	5.0	5.0
H_2/CO ratio	2.0	2.0
H_2/CO Flow (mL/min)	65	400
CO Space Velocity (v/v/h)	3620	3560
CO Conversion (%)	52.0	54.0
Carbon Selectivity (%)		
CH_4 (CO_2-free basis)	4.5	4.0
CO_2 (%)	42	40

Table 4

CO_2 Effects on Water-Gas Shift on the Catalyst (Zn/Fe = 0.1, 2 atomic% K, 1 atomic% Cu) at 235^oC and 21.4 atm)

CO_2 Pressure (atm)	CO_2/CO P Ratio	CO Conv. (%)	CO_2 Selectivity (%)	CO Conv. Rate to CO_2 (mmol/g-cat.h)	CO Conv. Rate to HC (mmol/g-cat.h)
0.0	0.00	26.1	22.6	7.0	23.8
1.0	0.15	28.4	22.6	7.6	26.3
1.5	0.23	28.2	22.2	7.4	26.8
2.2	0.33	26.3	20.0	6.2	25.3
3.5	0.53	25.7	18.5	5.6	25.3
4.5	0.68	26.6	16.7	5.2	27.8
8.0	1.21	26.7	13.7	4.3	31.5

Table 5

Comparison of Fischer-Tropsch Synthesis Results on Different Conditions on Fe-Based Catalyst (Zn/Fe = 0.1, 2 atomic% K, 1 atomic % Cu) and on 12.7 Wt.% Co/SiO_2 Catalyst

Catalyst	Fe-Based Catalyst			Co/SiO_2
Temperature, ^oC	235	220	270	200
Pressure (atm)	21.4	31.6	5.0	20.0
Catalyst weight (g)	0.4	0.4	0.4	1.5
H_2/CO ratio	2.0	2.0	2.0	2.0
Synthesis gas flow (mL/min)	53.0	29.0	53.0	20.0
CO space velocity (v/v/h)	2750	1510	2750	713
CO conversion (%)	43.8	42.6	44	49.0
CO conversion rate to HC (g/(g-cat.h))	0.45	0.28	0.37	0.13
CO conversion rate to HC (mol/(g-at Fe or Co.h))	2.7	1.8	2.3	2.0
CO conversion rate to HC (mL/(g-cat.h))	750	460	590	200
Carbon selectivity (%) (CO_2 free)				
CH_4	3.6	3.1	12.7	5.2
CO_2	30.6	17.5	43.0	0.4
C_3	7.5	7.2	13.6	1.9
C_4-C_{12}	32.6	32	49.7	21.2
C_{13}+	51.1	53	14.1	71.3
C_3 olefin/paraffin ratio	3.3	2.5	4.7	2.4

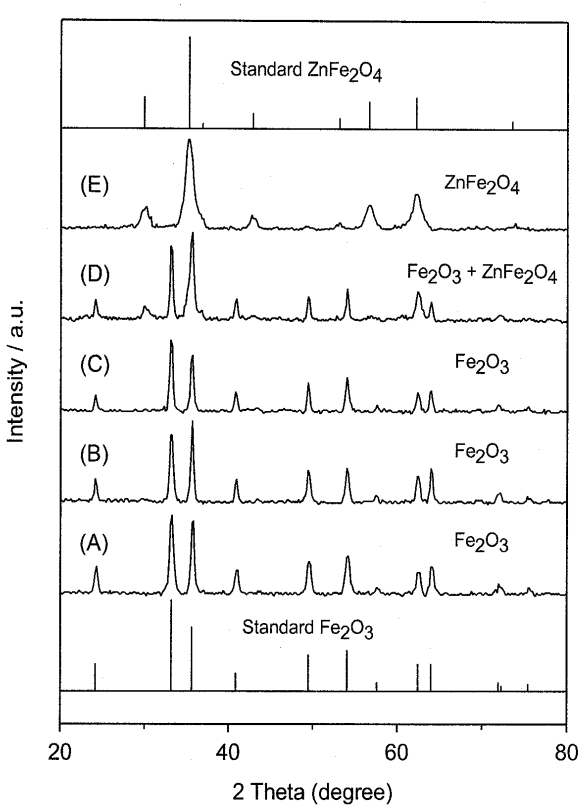

Figure 1. XRD of Fe-Zn-K-Cu samples with a Zn/Fe ratio of (A) 0, (B) 0.05, (C) 0.1, (D) 0.2 and (E) 0.4

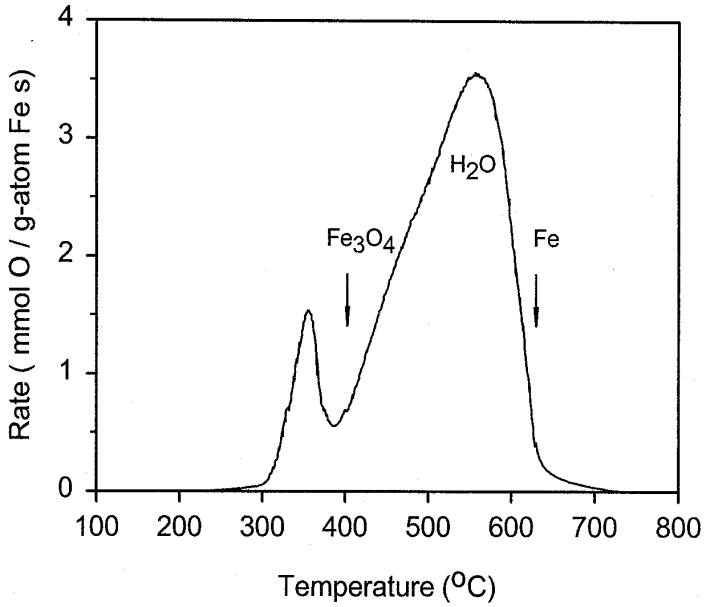

Figure 2. TPR of Fe_2O_3 in H_2 flow (0.2019 g Fe_2O_3; 100 cm^3/min., 20% H_2/Ar; 20^{o}C/min. ramping rate).

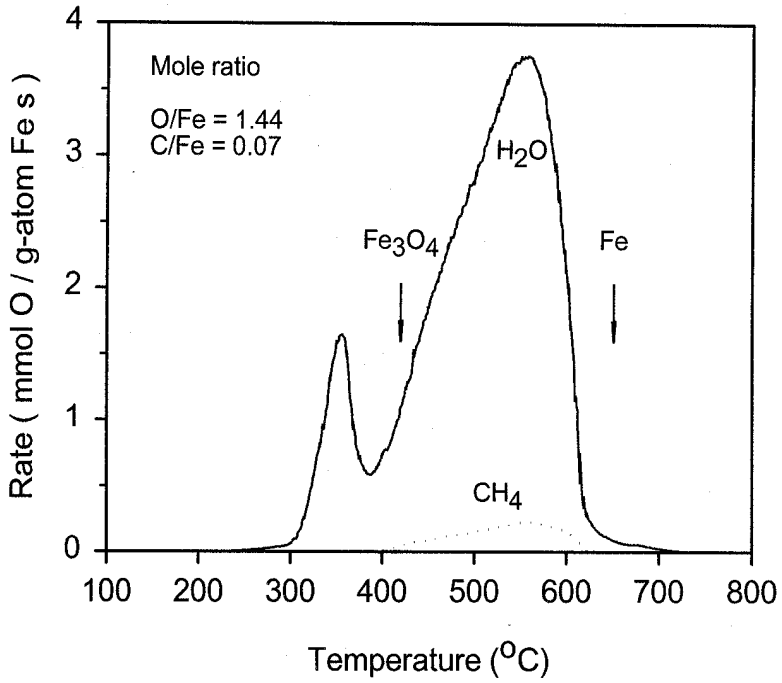

Figure 3. TPR of Fe_2O_3 in a mixture flow of $CH_4/4H_2$ (0.2022 g Fe_2O_3; 100 cm^3/min., 20% $_{CH4}$/H2; 20°C/min. ramping rate).

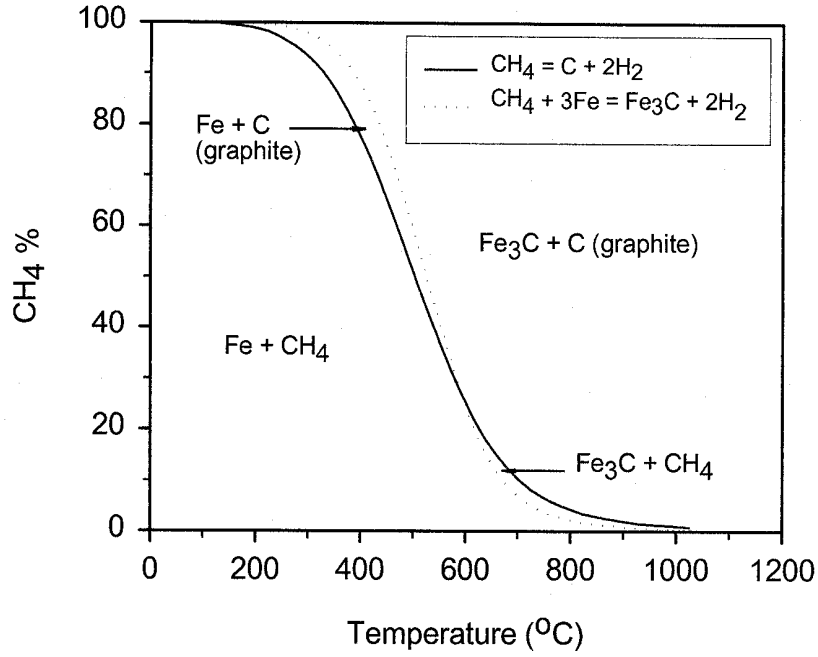

Figure 4. Equilibrium relationships at atm. pressure for the reaction CH_4 = C (graphite) + $2H_2$ and CH_4 + Fe = Fe_3C + $2H_2$ (calculation is based on the thermodynamic data provided by I. Barin, "Thermochemical Properties of Pure Substances," VCH, Weinheim, 3rd edition, 1995).

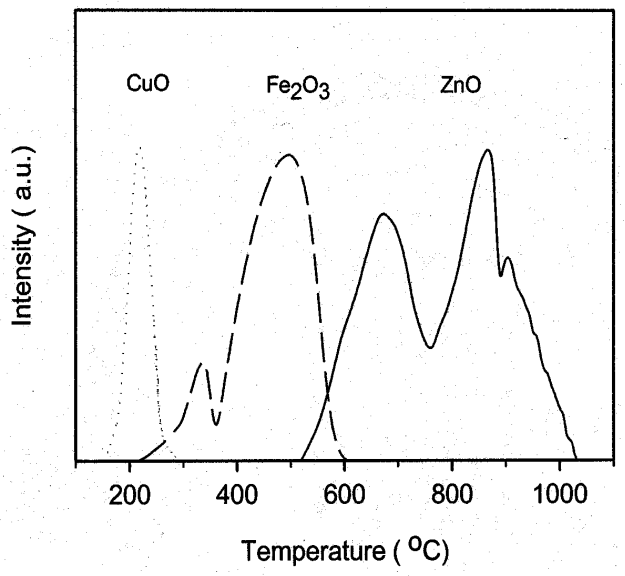

Figure 5. TPR of Fe, Zn and Cu oxides in H_2 (0.2 g samples; 10°C/min. ramping rate; 100 cm^3/min. 20% H_2/Ar).

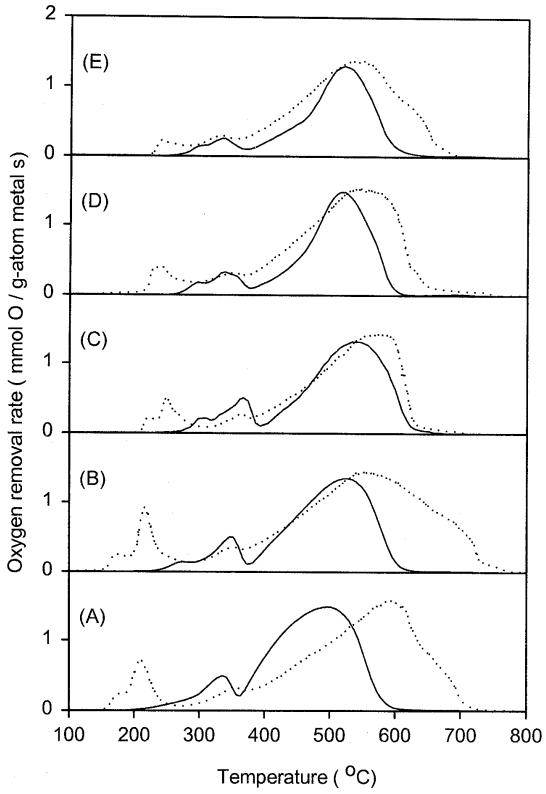

Figure 6. TPR of Fe-Zn and Fe-Zn-K-Cu samples in H_2 (——, Fe-Zn; ••••, Fe-Zn-K-Cu; 0.2 g samples; 10°C/min. ramping rate; 100 cm^3/min. 20% H_2/Ar).

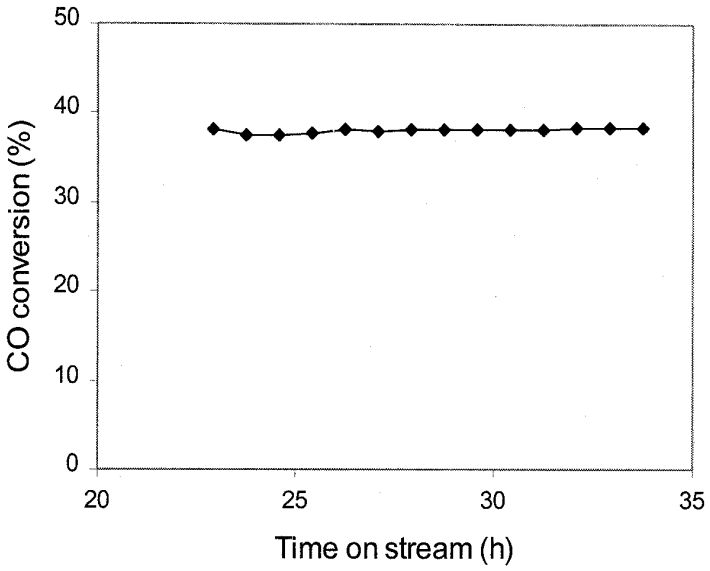

Figure 7. CO conversion as a function of time-on-stream on the catalyst (Zn/Fe = 0.07, 2 atomic% K, 1 atomic% Cu) at 235°C and 21.4 atm).

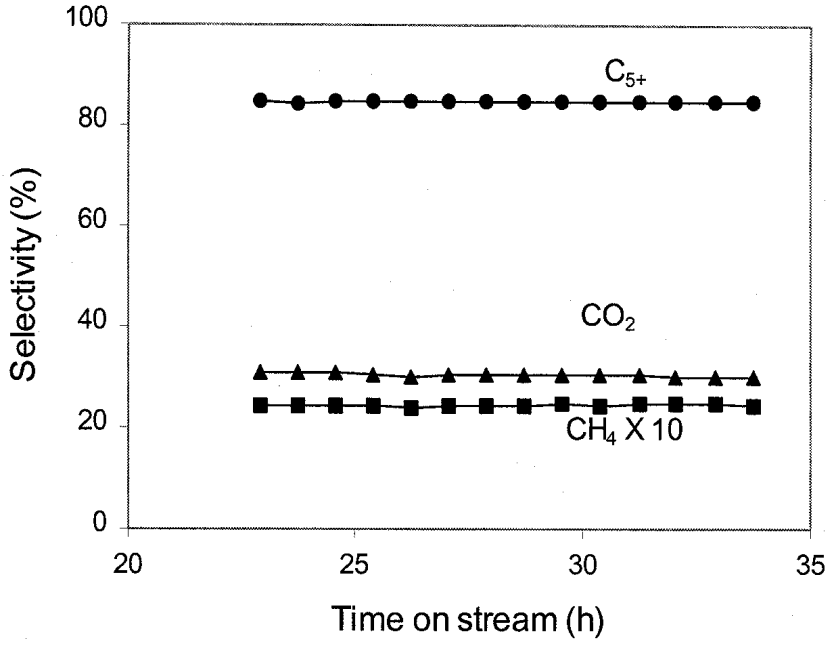

Figure 8. FTS selectivities as a function of time-on-stream on the catalyst (Zn/Fe = 0.07, 2 atomic% K, 1 atomic% Cu) at 235°C and 21.4 atm).

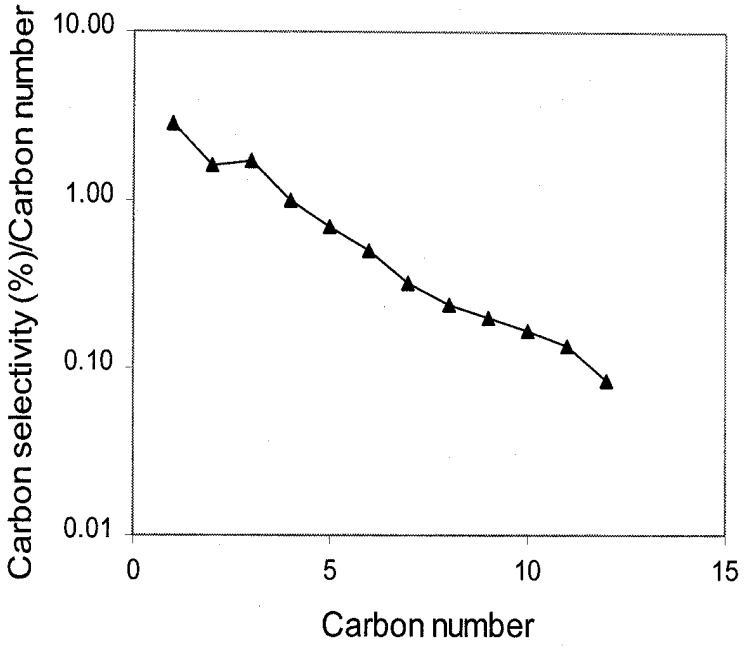

Figure 9. Carbon selectivity (%)/carbon number as a function of carbon number on the catalyst (Zn/Fe = 0.07, 2 atomic% K, 1 atomic% Cu) at 235°C and 21.4 atm).

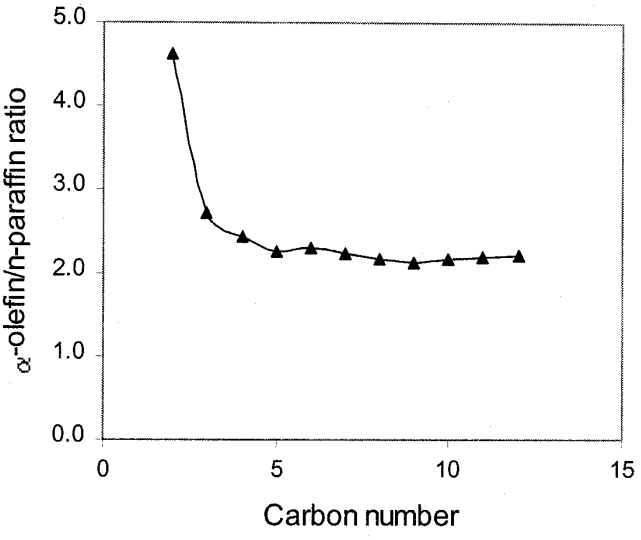

Figure 10. α-Olefin/n-paraffin ratio as a function of carbon number on the catalyst (Zn/Fe = 0.07, 2 atomic% K, 1 atomic% Cu) at 235°C and 21.4 atm).

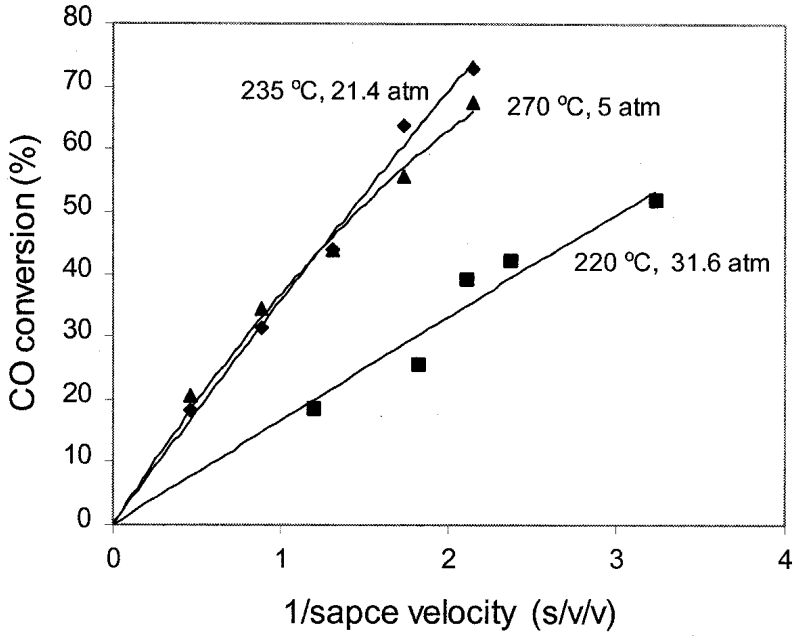

Figure 11. CO conversion as a function of reciprocal space velocity on the catalyst (Zn/Fe = 0.1, 2 atomic% K, 1 atomic% Cu).

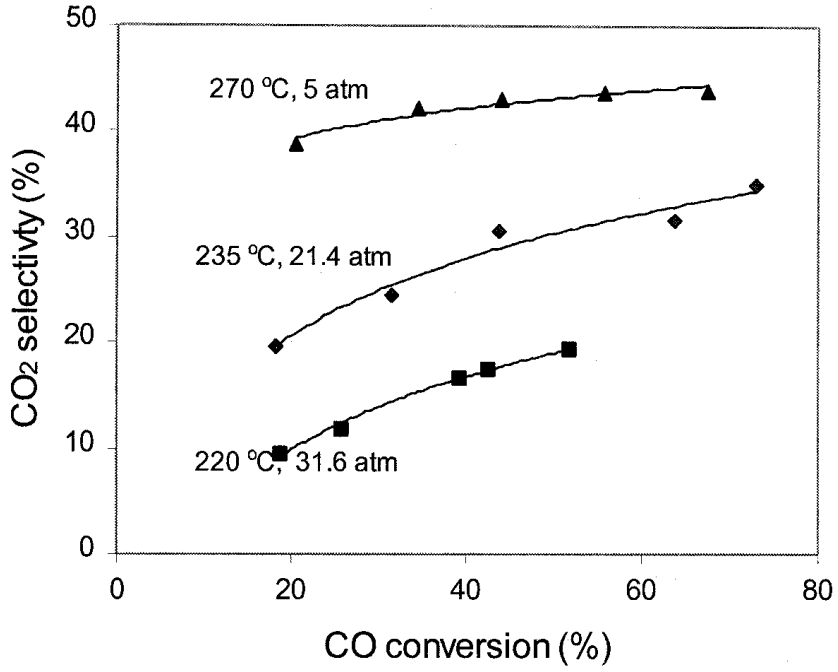

Figure 12. CO_2 selectivity as a function of CO conversion on the catalyst (Zn/Fe = 0.1, 2 atomic% K, 1 atomic% Cu).

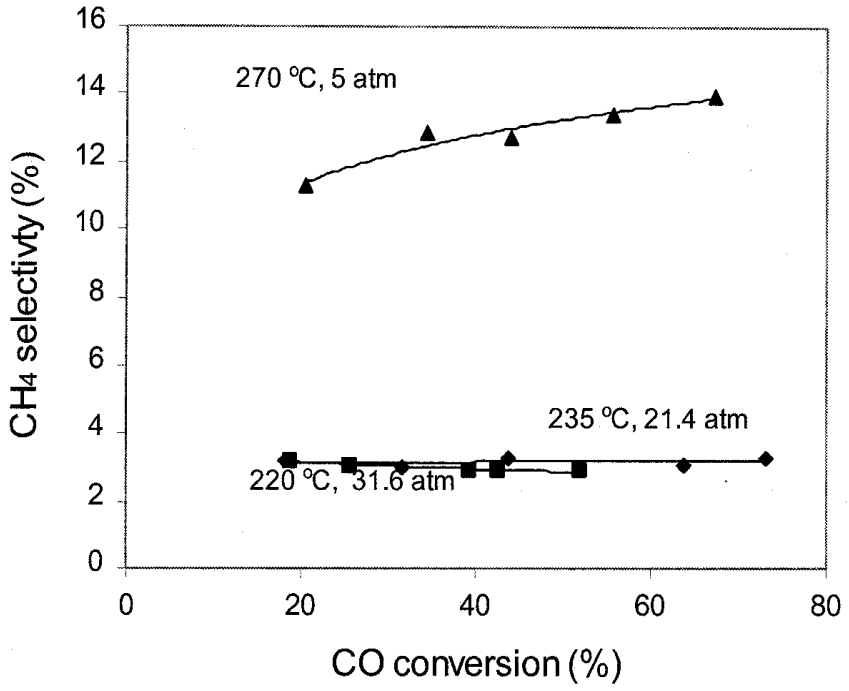

Figure 13. Methane selectivity as a function of CO conversion on the catalyst (Zn/Fe = 0.1, 2 atomic% K, 1 atomic% Cu).

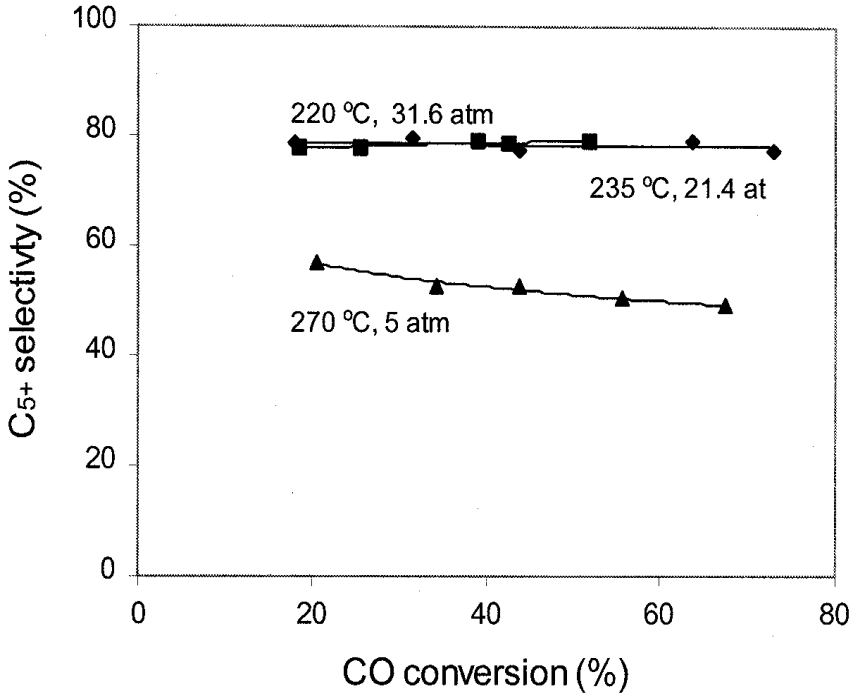

Figure 14. C_5+ selectivity as a function of CO conversion on the catalyst (Zn/Fe = 0.1, 2 atomic% K, 1 atomic% Cu).

II. APPENDIX

1. Schematic Diagram of Experimental Apparatus

1.1. Temperature-Programmed Surface Reaction (TPSR) Unit

1.2. Temperature-Programmed Reduction (TPR) Unit

1.3. Catalytic Microreactor Unit (CMRU) for FTS on Fe-based Catalysts

2. Peak Identification on Gas-Chromatograph (GC)

2.1. GC Conditions and Typical Products on Fe-based Catalysts

2.2. TCD Chromatogram with Peak Identification

2.3. Main Peaks on FID Chromatogram

2.4 FID Chromatogram with Retention Time

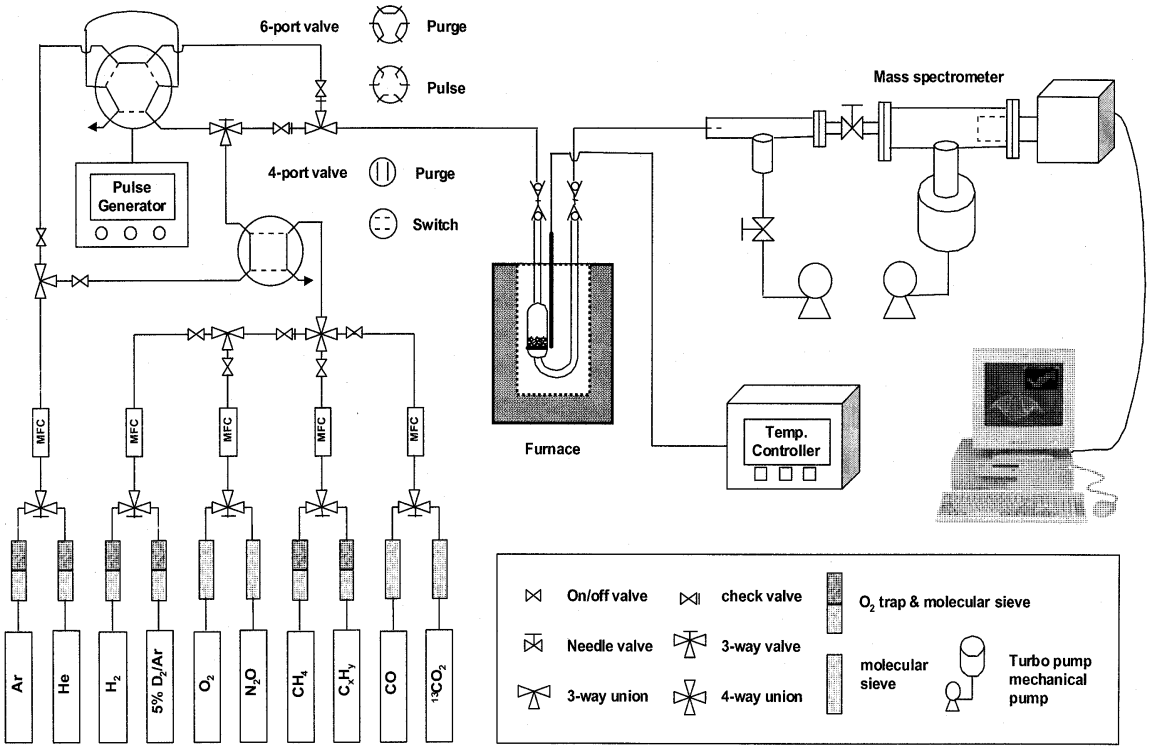

Appendix 1.1 Temperature-programmed surface reaction (TPSR) Unit.

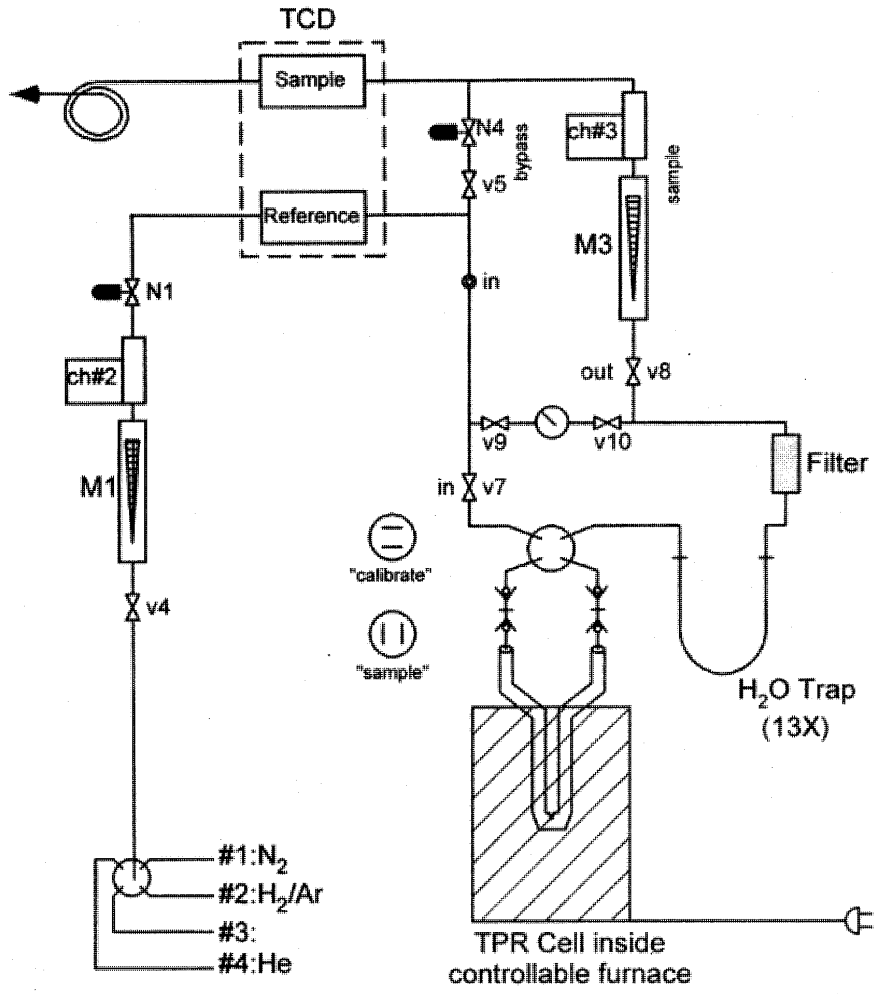

Temperature-reaction (TPR) Unit

Appendix 1.2 Temperature-programmed reaction (TPR) unit.

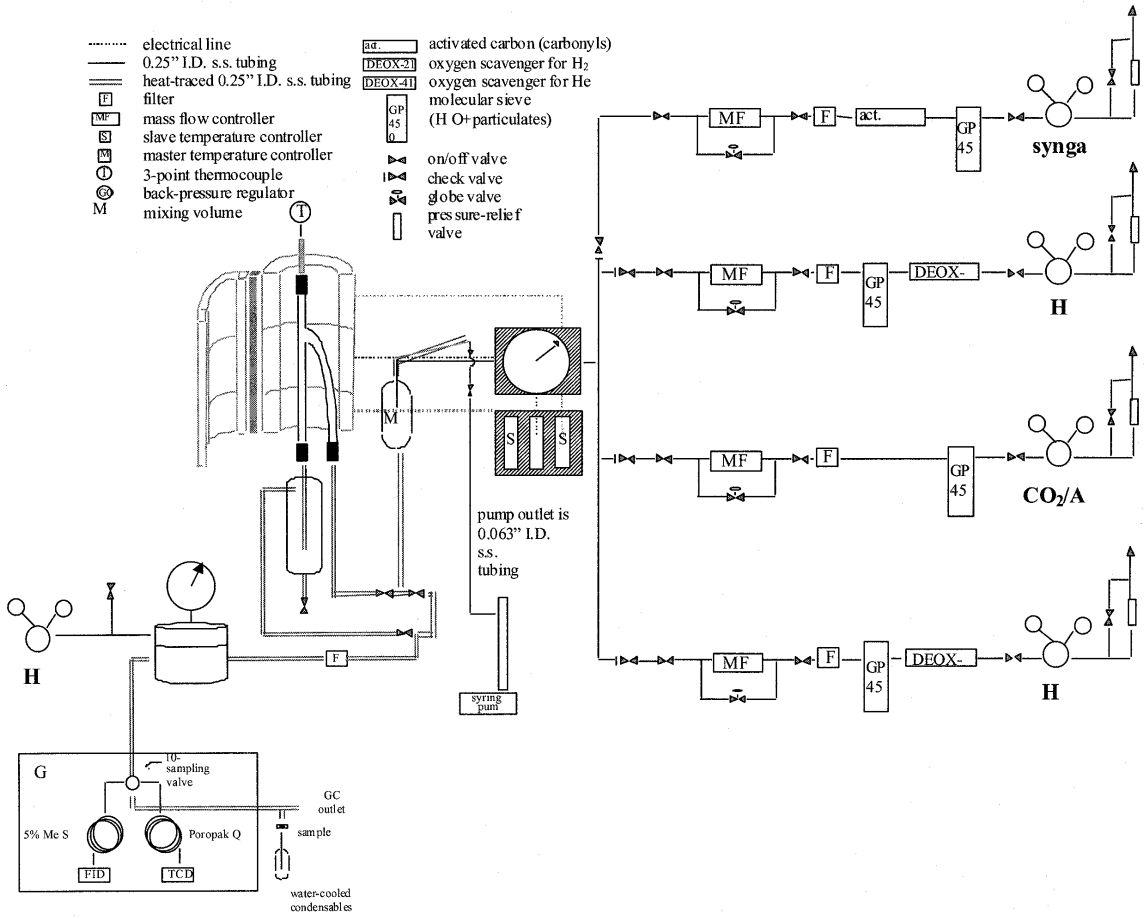

Appendix 1.3 Catalytic microreactor unit (CMRU) for FTS on Fe-based catalysts.

Appendix 3.1 Gas chromatograph conditions and typical products on Fe-based catalysts.

- Sample: Fe-Zn-K-Cu (Zn/Fe = 0.1, 2 at.% K and 1 at.% Cu); 0.4g.
- $CO/H_2/N_2$ = 31/62/7; 40 cm^3/min. flow rate.
- Pretreatment condition: 1 atm; 1^oC/ min. from ambient temperature to 250^oC, maintained at 250^oC for 0.5 h.
- Reaction condition: 270^oC; 5 atm.

TCD

Column		Porapak Q, 6' x 1/8" 80/100 mesh		
Oven	Initial Temperature (^oC)	-60	Initial Time (min)	3
	Ramping Rate (^oC/min)	10		
	Final Temperature (^oC)	240	Final Time (min)	10
Detector Temperature (^oC)		250	Injector Temperature (^oC)	250
Inlet Pressure (kPa)		400		
He flow rate (mL/min)		30	Reference flow rate (mL/min)	30

Index No.	Carbon Number	Products	Retention Time (min)
1		H_2	0.536
2		N_2	1.261
3	C1	CO	1.898
4	C1	CH_4	6.168
5	C1	CO_2	11.363
6	C2	C_2H_4	13.237
7	C2	C_2H_6	14.178
8	C3	C_3H_6	18.645
9	C3	$C_3H_8+H_2O$	19.345
10	C4	$C_4H_8+C_4H_{10}$	22.440

FID

Column		HP-1, crosslinked methyl silicone, 50m x 0.32 mm x 1.05µm		
Oven	Initial Temperature (^oC)	-60	Initial Time (min)	3
	Ramping Rate (^oC/min)	10		
	Final Temperature (^oC)	240	Final Time (min)	10
Detector Temperature (^oC)		250	Injector Temperature (^oC)	250
Inlet Pressure (psi)		23.2	Split Ratio	20:1
He flow rate (mL/min)		100	Make-up He flow rate (mL/min)	20
H_2 flow rate (mL/min)		30	Air flow rate (mL/min)	300

Index No.	Carbon Number	Products	Retention Time (min)
1	C1	CH_4	2.199
2	C2	C_2H_4	2.466
3	C2	C_2H_6	2.699
4	C3	C_3H_6	4.935
5	C3	C_3H_8	5.148
6	C2	CH_3CHO	7.741
7	C4	1-C_4H_8	8.695
8	C1	CH_3OH	8.776
9	C4	C_4H_{10}	8.977
10	C4	*Cis*-2-C_4H_8	9.372
11	C4	*Trans*-2-C_4H_8	9.833
12	C5	C_5H_{10}-isomer	10.817
13	C5	C_5H_{12}-isomer	11.325
14	C3	CH_3CH_2CHO	11.411
15	C5	1-C_5H_{10}	11.767
16	C5	C_5H_{10}-isomer	11.975
17	C5	1-C_5H_{12}	12.082
18	C5	C_5H_{10}-internal	12.320
19	C5	C_5H_{10}-internal	12.523
20	C5	C_5H_{10}-isomer	12.648
21	C6	C_6H_{12}-isomer	13.530
22	C6	C_6H_{12}-isomer	13.611
23	C6	C_6H_{12}-isomer	13.858
24	C6	C_6H_{14}-isomer	13.943
25	C4	$CH_3CH_2CH_2CH$	14.164
26	C6	C_6H_{14}-isomer	14.293

Index No.	Carbon Number	Products	Retention Time (min)
27	C6	1-C_6H_{12}	14.448
28	C6	1-C_6H_{14}	14.728
29	C6	C_6H_{12}-internal	14.849
30	C6	C_6H_{12}-internal	15.069
31	C7	C_7H_{14}-isomer	15.958
32	C7	C_7H_{14}-isomer	16.088
33	C7	C_7H_{14}-isomer	16.255
34	C7	C_7H_{16}-isomer	16.338
35	C7	C_7H_{16}-isomer	16.540
36	C7	C_7H_{14}-isomer	16.620
37	C7	C_7H_{14}-isomer	16.750
38	C7	1-C_7H_{14}	16.824
39	C7	1-C_7H_{16}	17.082
40	C7	C_7H_{14}-internal	17.182
41	C7	C_7H_{14}-internal	17.366
42	C8	C_8H_{16}-isomer	18.180
43	C8	C_8H_{16}-isomer	18.292
44	C8	C_8H_{16}-isomer	18.448
45	C8	C_8H_{18}-isomer	18.541
46	C8	C_8H_{16}-isomer	18.600
47	C8	C_8H_{18}-isomer	18.682
48	C8	C_8H_{16}-isomer	18.750
49	C8	C_8H_{16}-isomer	18.891
50	C8	1-C_8H_{16}	18.974
51	C8	1-C_8H_{18}	19.210
52	C8	C_8H_{16}-internal	19.290
53	C8	C_8H_{16}-internal	19.452
54	C9	C_9H_{18}-isomer	20.150
55	C9	C_9H_{18}-isomer	20.210
56	C9	C_9H_{18}-isomer	20.275
57	C9	C_9H_{18}-isomer	20.428
58	C9	C_9H_{20}-isomer	20.501
59	C9	C_9H_{20}-isomer	20.646
60	C9	C_9H_{18}-isomer	20.728
61	C9	C_9H_{18}-isomer	20.857
62	C9	1-C_9H_{18}	20.945
63	C9	C_9H_{18}-isomer	21.064
64	C9	1-C_9H_{20}	21.159
65	C9	C_9H_{18}-internal	21.210

Index No.	Carbon Number	Products	Retention Time (min)
66	C9	C_9H_{18}-internal	21.373
67	C10	$C_{10}H_{20}$-isomer	22.024
68	C10	$C_{10}H_{20}$-isomer	22.097
69	C10	$C_{10}H_{22}$-isomer	22.300
70	C10	$C_{10}H_{22}$-isomer	22.480
71	C10	$C_{10}H_{20}$-isomer	22.670
72	C10	1-$C_{10}H_{20}$	22.759
73	C10	$C_{10}H_{20}$-isomer	22.856
74	C10	1-$C_{10}H_{22}$	22.960
75	C10	$C_{10}H_{20}$-internal	23.000
76	C10	$C_{10}H_{20}$-internal	23.159
77	C11	$C_{11}H_{22}$-isomer	23.750
78	C11	$C_{11}H_{22}$-isomer	23.828
79	C11	$C_{11}H_{22}$-isomer	23.940
80	C11	$C_{11}H_{24}$-isomer	24.002
81	C11	$C_{11}H_{24}$-isomer	24.050
82	C11	$C_{11}H_{24}$-isomer	24.172
83	C11	$C_{11}H_{22}$-isomer	24.259
84	C11	$C_{11}H_{22}$-isomer	24.355
85	C11	1-$C_{11}H_{22}$	24.445
86	C11	$C_{11}H_{22}$-isomer	24.500
87	C11	1-$C_{11}H_{24}$	24.629
88	C11	$C_{11}H_{22}$-internal	24.814
89	C12	$C_{12}H_{24}$-isomer	25.360
90	C12	$C_{12}H_{24}$-isomer	25.461
91	C12	$C_{12}H_{26}$-isomer	25.520
92	C12	$C_{12}H_{26}$-isomer	25.580
93	C12	$C_{12}H_{24}$-isomer	25.650
94	C12	$C_{12}H_{26}$-isomer	25.760
95	C12	$C_{12}H_{24}$-isomer	25.931
96	C12	1-$C_{12}H_{24}$	26.013
97	C12	$C_{12}H_{24}$-isomer	26.070
98	C12	1-$C_{12}H_{26}$	26.181
99	C12	$C_{12}H_{24}$-isomer	26.250
100	C12	$C_{12}H_{24}$-internal	26.362
101	C13	$C_{13}H_{26}$-isomer	26.863
102	C13	$C_{13}H_{28}$-isomer	26.980
103	C13	$C_{13}H_{28}$-isomer	27.068
104	C13	$C_{13}H_{28}$-isomer	27.134

Index No.	Carbon Number	Products	Retention Time (min)
105	C13	$C_{13}H_{26}$-isomer	27.234
106	C13	$C_{13}H_{26}$-isomer	27.240
107	C13	$C_{13}H_{26}$-isomer	27.400
108	C13	1-$C_{13}H_{26}$	27.479
109	C13	$C_{13}H_{26}$-isomer	27.510
110	C13	1-$C_{13}H_{28}$	27.631
111	C13	$C_{13}H_{26}$-isomer	27.780
112	C13	$C_{13}H_{26}$-internal	27.809
113	C14	$C_{14}H_{28}$-isomer	28.210
114	C14	$C_{14}H_{30}$-isomer	28.402
115	C14	$C_{14}H_{30}$-isomer	28.520
116	C14	$C_{14}H_{28}$-isomer	28.622
117	C14	$C_{14}H_{28}$-isomer	28.688
118	C14	1-$C_{14}H_{28}$	28.854
119	C14	1-$C_{14}H_{30}$	28.992
120	C14	$C_{14}H_{28}$-internal	29.164
121	C15	$C_{15}H_{30}$-isomer	29.634
122	C15	$C_{15}H_{32}$-isomer	29.742
123	C15	$C_{15}H_{32}$-isomer	29.925
124	C15	$C_{15}H_{30}$-isomer	30.011
125	C15	1-$C_{15}H_{30}$	30.147
126	C15	1-$C_{15}H_{32}$	30.273
127	C15	$C_{15}H_{30}$-internal	30.476
128	C16	$C_{16}H_{32}$-isomer	30.869
129	C16	$C_{16}H_{34}$-isomer	31.003
130	C16	$C_{16}H_{34}$-isomer	31.159
131	C16	$C_{16}H_{32}$-isomer	31.261
132	C16	1-$C_{16}H_{32}$	31.367
133	C16	1-$C_{16}H_{34}$	31.483
134	C16	$C_{16}H_{32}$-isomer	31.655
135	C16	$C_{16}H_{32}$-internal	31.726

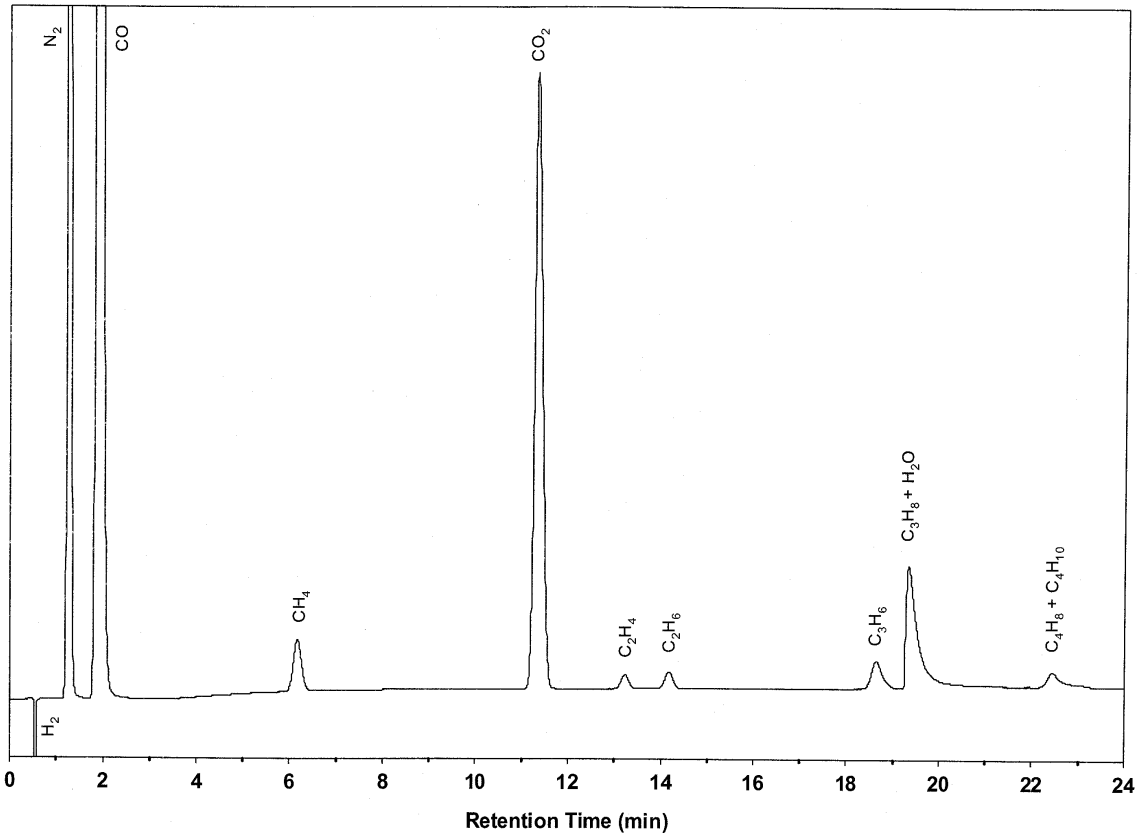

Appendix 2.2 TCD chromatogram with peak identification.

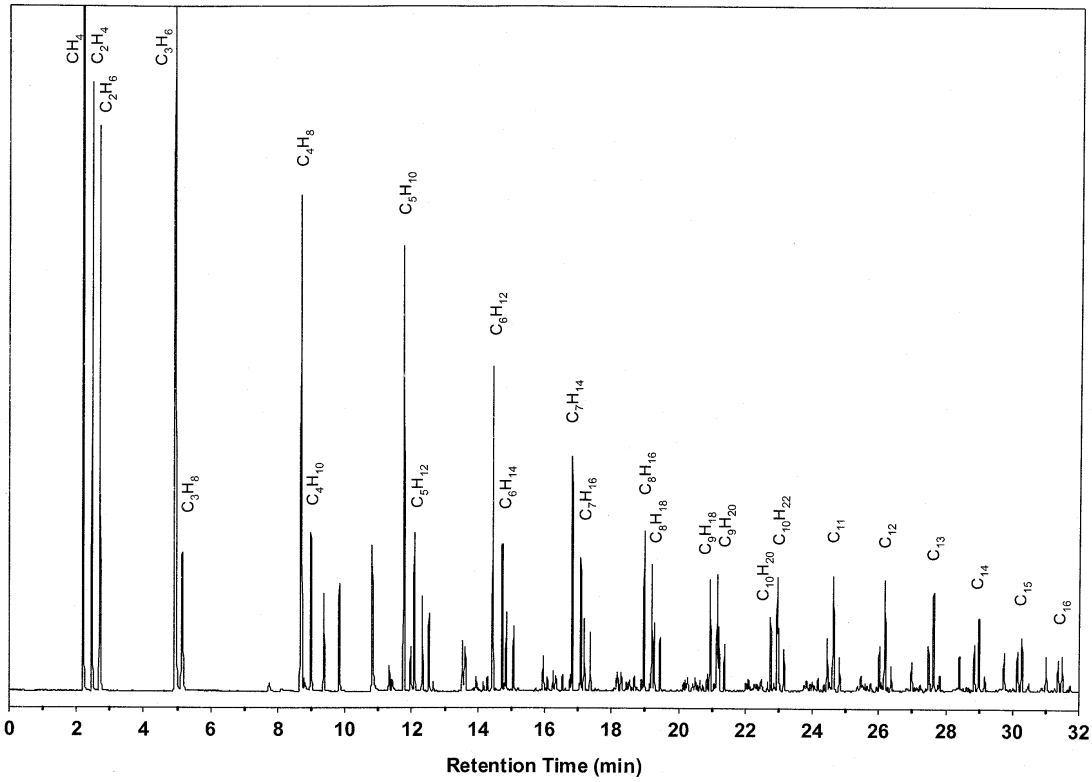

Appendix 2.3 Main peaks on FID chromatogram.

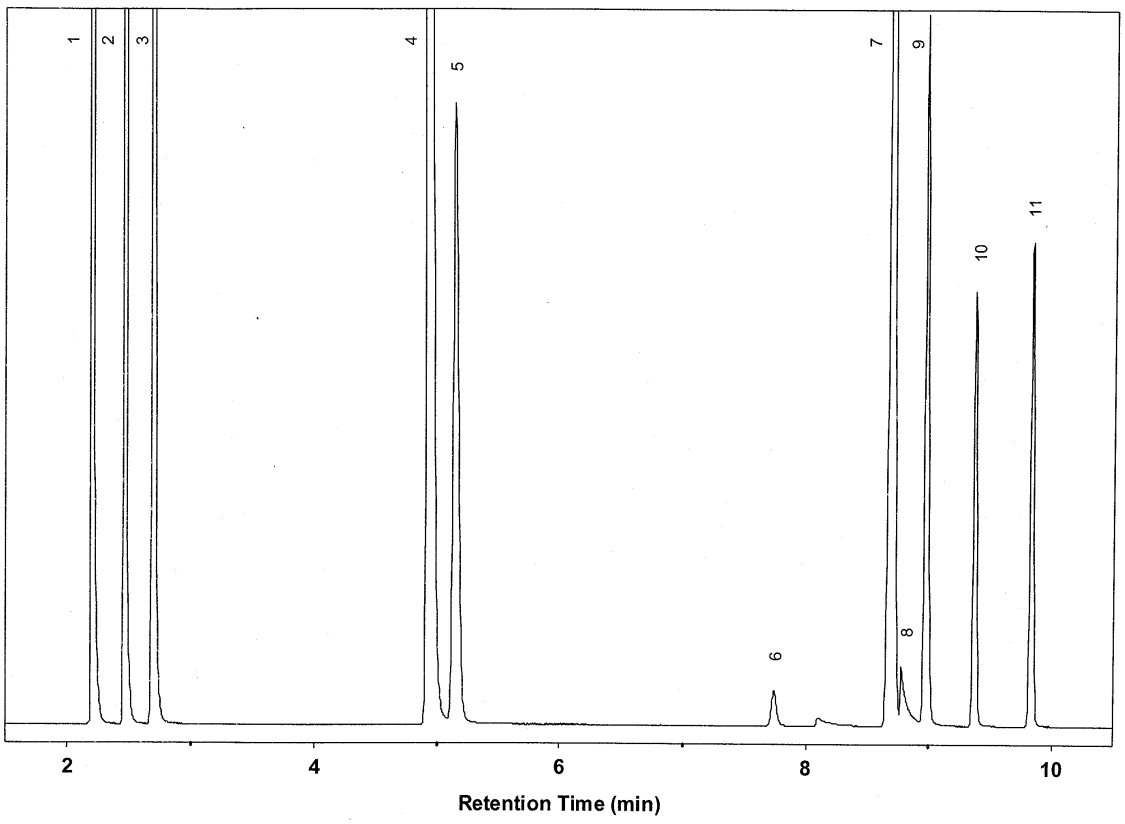

Appendix 2.4 FID chromatogram with retention time.

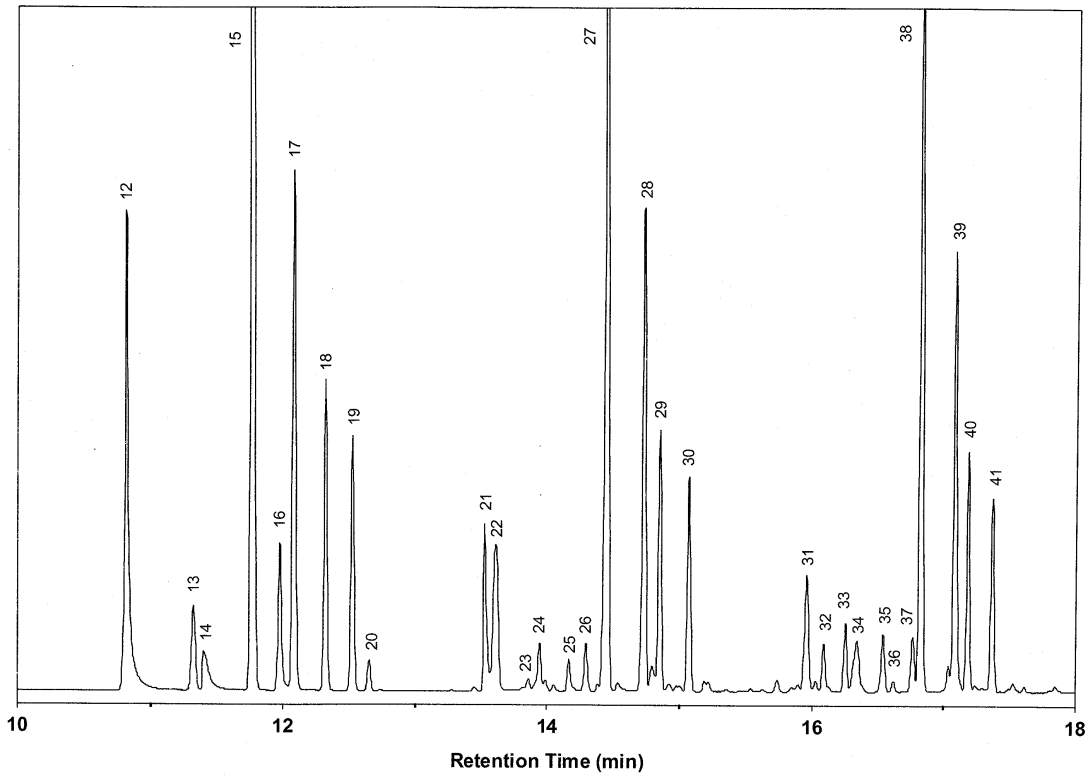

Appendix 2.4 (continued)

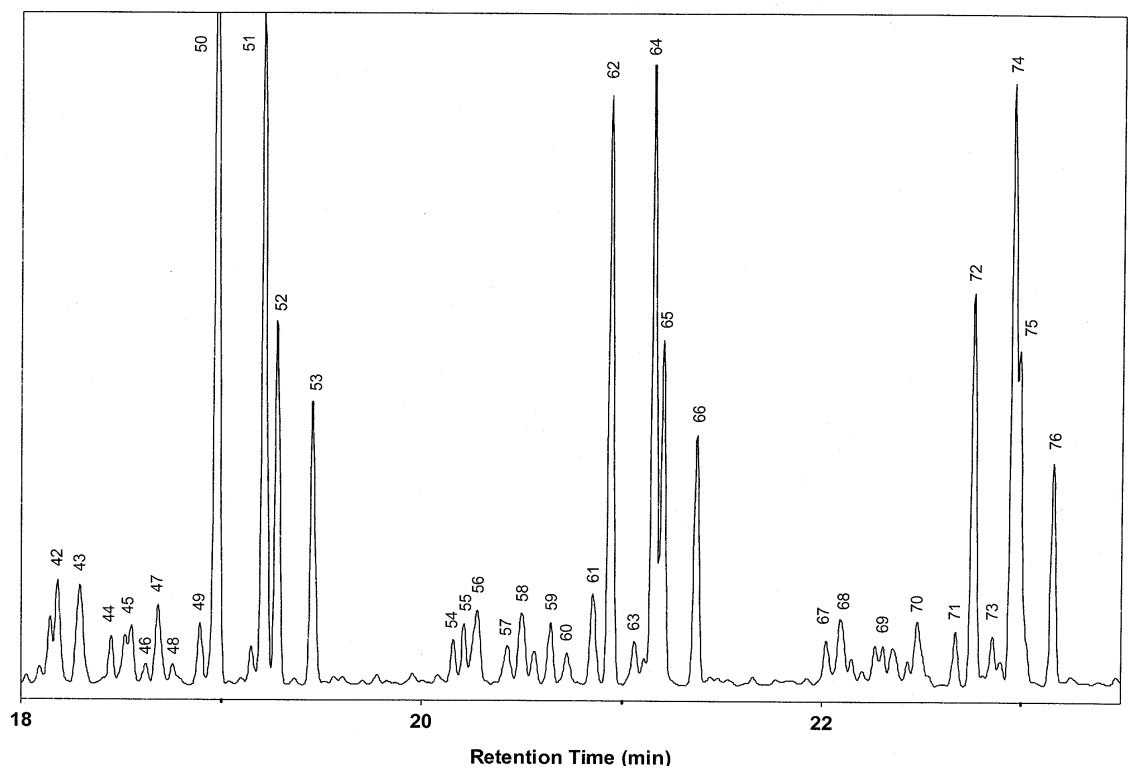

Appendix 2.4 (continued)

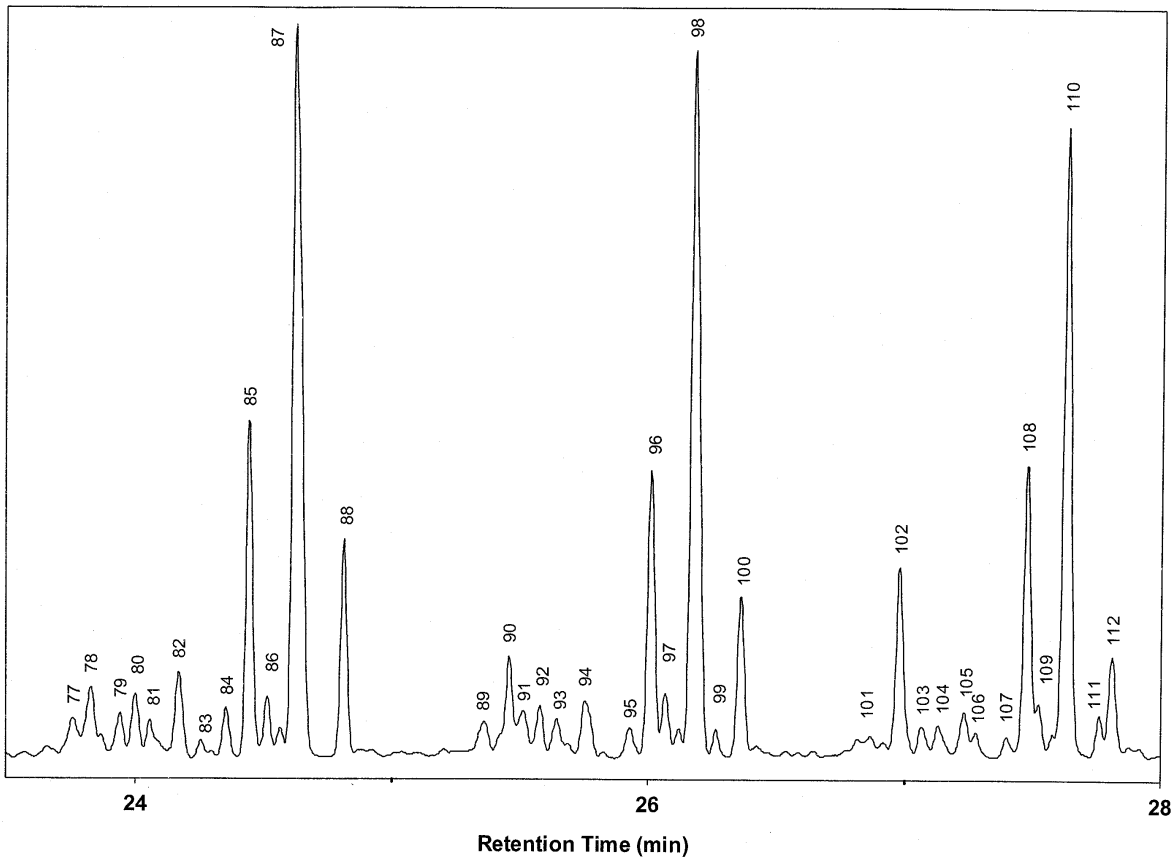

Appendix 2.4 (continued)

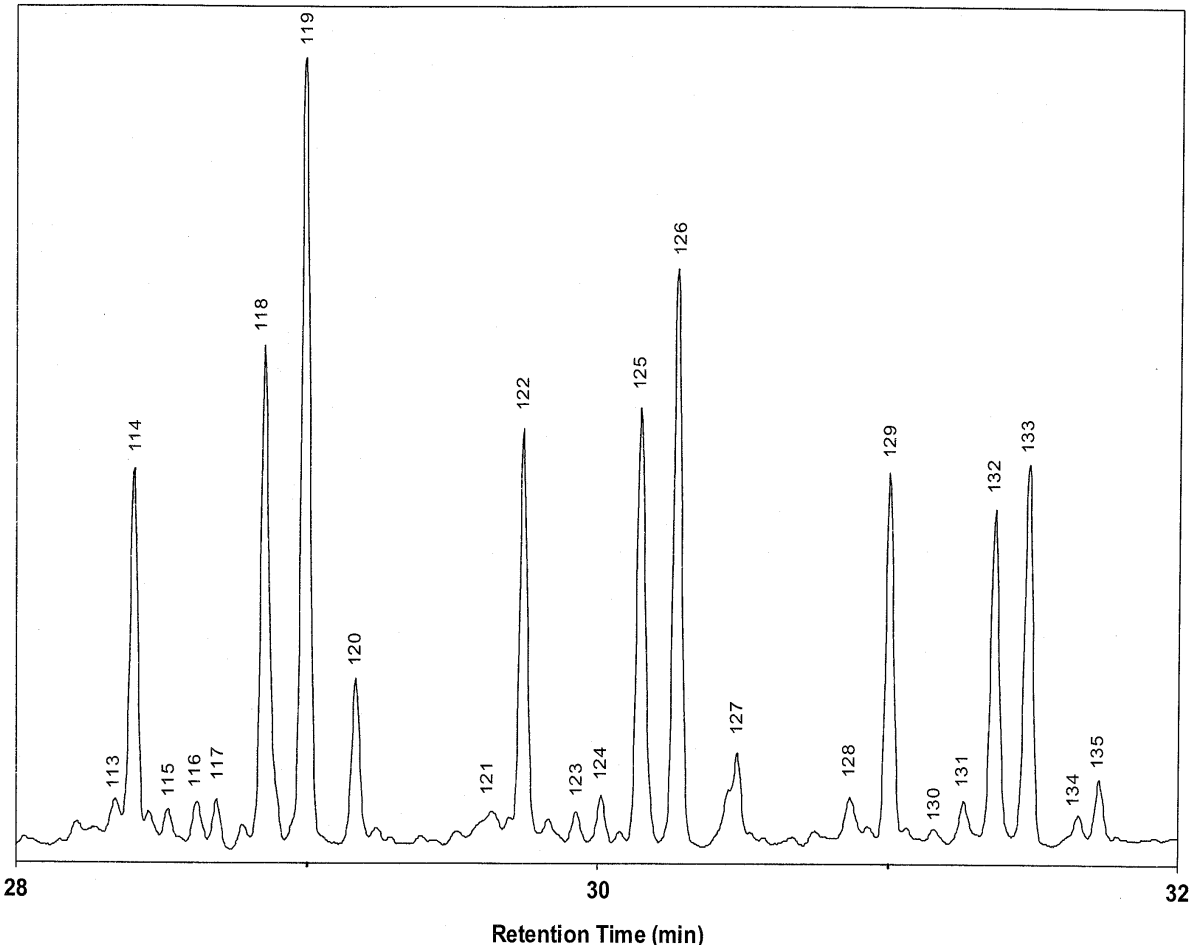

Appendix 2.4 (continued)

Task 12. Reporting/Project Management

Three monthly and one quarterly reports have been completed. The first quarterly meeting between Dr. B. H. Davis and Dr. E. Iglesia was held on December 18, 1998 at the University of California, Berkeley. The notes from that meeting are given below.

QUARTERLY MEETING - FISCHER-TROPSCH PI'S

The first of the quarterly meetings for the contract "Technology Development for Iron and Cobalt Fischer-Tropsch Catalysts," DE-FC26-98FT40308 was held at the Chemical Engineering Department, University of California, Berkeley, on December 18, 1998.

Dr. Burt Davis provided an overview of the results obtained from work conducted with iron Fischer-Tropsch catalysts at the Center for Applied Energy Research on previous DOE contracts. This included results for: (1) the preparation and activation of iron catalysts, (2) characterization of fresh and used catalysts, (3) catalyst aging studies, and (4) the impact of promoters on the activity, stability and selectivity of the catalysts.

Four members of Professor Iglesia's research group described results that they have obtained to date.

Dr. Senzi Li presented data for the preparation of a series of catalysts composed of combinations of Fe, Zn, K and Cu. The catalysts have been prepared by coprecipitation of Zn and Fe hydrous oxides to cover Zn/Fe ratios ranging from 0 to 0.4. Temperature programmed reduction has been used to characterize the reduction of the catalyst using hydrogen and carbon monoxide. In the reduction with carbon monoxide, the data indicate that the material contains much more oxygen than would be expected

following treatments to 600 oC. Oxygen isotopic tracer studies will be conducted to define the amount of oxygen retained by the catalytic material following various heat treatments.

Dr. Wei Li provided an overview of the modeling he is doing before conducting transient isotopic tracer studies of the number of sites and the FT mechanism. The isotopic transients will include switching from 13CO to 12CO,H2 to D2, and H2O to D2O.

Dr. Anwu Li described work he has conducted in a fixed-bed reactor using catalysts containing Fe, Zn, K and Cu. The work to date has focused on conducting the synthesis with a range of CO2 pressures in the synthesis gas fed to the reactor. The work is to define whether the presence of high partial pressures of CO2 will decrease the contribution of the water gas shift to the synthesis. The early results suggest that the partial pressure of CO2 required to stop water gas shift reactions may be too high to be of practical use. Thus CO2 is likely to have to recycled to the synthesis gas generation rather than just to the FT reactor.

Dr. Mai Tu described a study of the effect of water on FTS rate and selectivity on generic cobalt-silica catalysts. It was found that the silica with wide pores exhibits a promoting effect of water on FTS reaction rates, but that Coon small-pore silica did not. All catalysts, however, showed an increase in product molecular weight and in olefin content with increasing water partial pressure. Bed residence time effects were also investigated. On catalysts showing a promotion effect of water, the CO conversion increases faster than linearly with increasing bed residence time and the C5+ selectivity and product paraffin content also increase with increasing conversion and bed residence time. In contrast to the effect of water on FTS rates, which is observed only

with some supports, the bed residence time and water effects on selectivity were observed on all silica-supported catalysts, irrespective of the pore structure of the silica support.

COOPERATIVE WORK DURING THE NEXT QUARTER

1. CAER personnel will provide Prof. Iglesia with a sample of a catalyst containing Fe,Si,K, and Cu that has been tested in the autoclave reactors for long periods of time and where samples have been withdrawn for characterization as a function of time on stream. This sample will be utilized by the Berkeley group in their fixed bed reactor to obtain the chemical state of iron in the catalyst and to observe changes during synthesis utilizing EXAFS technique. CAER personnel will also conduct a run in the CSTR using the same reaction conditions as used by the Berkeley team: 270 oC and 5 atm, 230oC, 30 atm and 250oC, 20 atm.
2. Work at the CAER using the Zn,Fe containing catalyst with 14CO2 isotopic tracers to study the reverse water gas shift reaction will be combined with the data obtained at Berkeley in order to develop a better understanding of the extent of the extent to which CO2 partcipates in chain initiation and growth and of whether reverse water gas shift reactions can be used to minimize CO2 formation during FTS on Fe-based catalysts.
3. CAER will utilize their high-temperature gas chromatograph to analyze wax samples generated at Berkeley.
4. CAER will provide the Berkeley group with samples of an unpromoted iron catalyst that has been characterized using M`ssbauer spectroscopy.

5. In order to maintain some common basis for reporting catalyst activity and productivity, each group will include data for feed conversion rates in moles CO/g atom metal-h and hydrocarbon productivity of g hydrocarbon/g atom metal-h.
6. CAER will provide Berkeley with a sample budget sheet and the phone number and e-mail of the person at UKRF who does the invoicing of DOE.
7. The next meeting between the PIs will take place in Lexington, probably at a convenient in March-April, 1999.

   Several wax samples have been analyzed by CAER for UC/B.